Journal of Power Sources 195 (2010) 2220–2223

Contents lists available at ScienceDirect

Journal of Power Sources

journal homepage: www.elsevier.com/locate/jpowsour

Short communication

Fabrication and characterization of a $Ba_{0.5}Sr_{0.5}Co_{0.8}Fe_{0.2}O_{3-\delta}$—Gadolinia-doped ceria cathode for an anode-supported solid-oxide fuel cell

Wei-Xin Kao, Maw-Chwain Lee*, Tai-Nan Lin, Chun-Hsiu Wang, Yang-Chuang Chang

Chemical Engineering Division, Institute of Nuclear Energy Research, No. 1000, Wunhua Rd., Jiaan Village, Longtan Township, Taoyuan County 32546, Taiwan, ROC

ARTICLE INFO

Article history:
Received 11 September 2009
Received in revised form 20 October 2009
Accepted 20 October 2009
Available online 30 October 2009

Keywords:
Solid-oxide fuel cell
BSCF
AC-impedance

ABSTRACT

$Ba_{0.5}Sr_{0.5}Co_{0.8}Fe_{0.2}O_{3-\delta}$ (BSCF) and gadolinia-doped ceria (GDC) were synthesized via a glycine-nitrate process (GNP). A cubic perovskite of BSCF was observed by X-ray diffraction (XRD) at a calcination temperature above 950 °C. An anode-supported solid-oxide fuel cell was constructed from the porous NiO + YSZ as the anode substrate, the yittria-stabilized zirconia (YSZ) as the electrolyte, and the porous BSCF-GDC layer as the cathode with a GDC barrier layer. For the performance test, the maximum power density was 191.3 mW cm^{-2} at a temperature of 750 °C with H_2 fuel and air at flow rates of 335 and 670 sccm, respectively. According to the AC-impedance data, the charge-transfer resistances of the electrodes were 0.10 and 1.59 Ω cm^2, and the oxygen-reduction and oxygen-ion diffusion resistances were 0.69 and 0.98 Ω cm^2 at 750 and 600 °C, respectively. SEM microstructural characterization indicated that the fuel cell as fabricated exhibited good compatibility between cathode and electrolyte layers.

1. Introduction

Solid-oxide fuel cells (SOFCs) have the advantages of high-efficiency energy conversion, low polluting emissions, and high orientation of fuels. However, high operating temperatures of over 800 °C are required for conventional SOFCs to maintain high oxygen-ionic conductivity. A key obstacle to lowering the operating temperature of SOFCs is the poor activity of traditional cathode materials [1]. In an anode-supported SOFC, the cathode polarization resistance is the main contributor to overall cell resistance at intermediate operating temperatures. Thus, to develop intermediate-temperature SOFCs (IT-SOFCs) it is essential to introduce novel cathode materials with high catalytic activities to enhance the generation rate of oxygen ions and to decrease the operating temperature.

Key characteristics of a good cathode material with enhanced electrochemical performance include the following: (1) a high rate of oxygen diffusion through the material to assure the rapid diffusion of oxygen; (2) a high electronic conductivity; (3) a high oxygen-ion conductivity; (4) a high catalytic activity for the reduction of oxygen; and (5) a suitable thermal-expansion coefficient to assure chemical and mechanical compatibility between electrode materials and the electrolyte [2–4]. The cobalt- or iron–cobalt-based perovskites are known to have better performance than that of the typical LSM-YSZ composite as cathode materials [5]. Strontium-doped lanthanum manganites ($La_{1-x}Sr_xMnO_{3-\delta}$; LSMs) have been used extensively as cathode materials in YSZ-based SOFCs due to their matching thermal-expansion coefficients, assuring mechanical compatibility and high electronic conductivity. However, LSMs have very poor oxide-ion conduction. Strontium-doped lanthanum cobaltites ($La_{1-x}Sr_xCoO_{3-\delta}$; LSCs) and their ion-substituted derivatives ($La_{1-x}Sr_xCo_yFe_{1-y}O_{3-\delta}$; LSCFs) are known to have high catalytic activity for the reduction of oxygen and high electronic conductivity. However, the large thermal-expansion coefficient of LSC results in the problem of mechanical compatibility. The Co-based pervoskite material $Sm_xSr_{1-x}CoO_{3-\delta}$ (SSC) also has high electronic conductivity [3,6]. $Ba_{1-x}Sr_xCo_yFe_{1-y}O_{3-\delta}$ (BSCF) gives excellent performance as the cathode for a reduced-temperature (600 °C) SOFC due to its high rate of oxygen diffusion through the material. In spite of the low electronic conductivity of BSCF, it has some advantages in the lower electrochemical surface-exchange resistance [7] and lower cost. The oxygen-reduction in BSCF occurs not only on the triple-phase boundary (TPB), but also proceeds on the surface of the electrode. Therefore, the diffusion of the oxygen ions from the electrode surface to the electrode/electrolyte interface can be improved. This phenomenon can be seen as an extension of the TPB [8]. There are many routes to synthesize BSCF powder, such as solid-state reaction [9,10], the citrate-EDTA method [10], and the glycine-nitrate process [11].

However, the BSCF cathode is not compatible with zirconia-based electrolyte because of their chemical interaction to produce an interfacial-insulating layer and reduce the catalytic activity of the electrode [6,12]. Accordingly, the BSCF cannot be directly

* Corresponding author. Tel.: +886 3 4711400x5930; fax: +886 3 4711411.
E-mail address: mclee@iner.gov.tw (M.-C. Lee).

0378-7753/$ – see front matter © 2009 Elsevier B.V. All rights reserved.
doi:10.1016/j.jpowsour.2009.10.057

applied onto a YSZ electrolyte. Gadolinia-doped ceria (GDC) is known to be chemically compatible with the BSCF, and possesses a higher ionic conductivity than that of the YSZ electrolyte [6,12–14]. Therefore, the GDC can be coated onto a YSZ electrolyte as a barrier layer to prevent the interaction between the BSCF cathode and YSZ electrolyte. BSCF has a high thermal-expansion coefficient (TEC) which does not match the GDC barrier layer, with a lower TEC value. This disadvantage can be overcome by the addition of GDC to BSCF to adjust the TEC of the BSCF cathode. In the study by Wang et al. [15], the cell with a BSCF-GDC-Ag electrode as the cathode and GDC as the electrolyte exhibited a good compatibility in the cell structure. The area-specific resistance (ASR) for the cathode composed of 70 wt.% BSCF and 30 wt.% GDC was lower than those of other GDC contents tested for the BSCF cathode. The average TEC of BSCF can be reduced to $16.11 \times 10^{-6}\,K^{-1}$ by the introduction of 30 wt.% GDC for temperatures between 30 and 850 °C.

In this study, a symmetrical fuel cell with Ni-YSZ as the anode, YSZ as the electrolyte, GDC as the barrier layer, and BSCF-GDC as the cathode was fabricated. The BSCF and GDC powders were individually synthesized via a glycine-nitrate process (GNP). The phase compositions of the BSCF powders were characterized by XRD. The performance and AC-impedance tests of the single cell were also evaluated.

2. Experimental

2.1. Synthesis of powders

The BSCF powders were synthesized using the glycine-nitrate process. In this case, stoichiometric amounts of $Ba(NO_3)_2$ (SHOWA, 99%), $Sr(NO_3)_2$ (Merck, 99%), $Co(NO_3)_2{\cdot}6H_2O$ (SHOWA, 98%), and $Fe(NO_3)_3{\cdot}9H_2O$ (Merck, 99%) were used as the starting raw materials. Metal nitrates were dissolved in distilled water and then the glycine was added to the solution. The mixture was heated on a hot plate, evaporated to a viscous gel, and ignited with a flame, resulting in a BSCF ash of a dark-gray color. The ash was afterwards calcined at temperatures ranging from 400 to 1000 °C for 4 h to remove carbon residues remaining in the ash. The GDC powders were synthesized by the same method. Powders of $Ce(NO_3)_3{\cdot}6H_2O$ (Merck, 98.5%) and $Gd(NO_3)_3{\cdot}5H_2O$ (Acros, 99.9%) were used as starting materials and the GDC powders were calcined at 1300 °C for four hours.

2.2. Fabrication of the single cell

An anode-supported solid-oxide fuel cell with a structure of Ni-YSZ (anode) |YSZ (electrolyte)|GDC (buffer-layer)|BSCF-GDC (cathode) was fabricated with an active area of ~16 cm^2. The anode substrate was prepared via a tape-casting process and sintered at 1400 °C for four hours. The casting was performed using a bench-scale commercial tape-casting system (ECS, Model CS-8). The YSZ electrolyte was elaborated onto the anode substrate via a spin-coating method and sintered at 1400 °C for four hours. The GDC barrier layer was printed onto the YSZ electrolyte layer via a screen printer and sintered at 1250 °C for four hours. The cathode composite of 70 wt.% BSCF and 30 wt.% GDC was then printed onto the GDC barrier layer by a screen printer.

2.3. Characterizations of materials and cell

The thermal-decomposition behavior of BSCF was examined by thermo-gravimetric analysis (TGA, Linseis, L81/1750) with a heating rate of 5 °C min^{-1} in air or N_2. The phase identification of BSCF was performed by X-ray diffraction (XRD, Bruker, D8 advance) using CuKα radiation in the range of $2\theta = 20–80°$ with a scanning speed of 1° $(2\theta)\,min^{-1}$. The morphology of the cross-sections of the single cell was observed via field-emission scanning-electron microscopy (FE-SEM, Hitachi, S-4800). The cell was set in a purpose-built measurement station for the electrochemical property investigations. The cell performance was measured at 800 °C with an inlet fuel of pure H_2 and an inlet oxidant of air. The flow rates of H_2 and air were fixed at 335 and 679 ml min^{-1}, respectively. AC-impedance measurement was performed using an impedance analyzer (Solartron 1260) under an open-circuit condition at frequencies from 10^5 to 10^{-2} Hz.

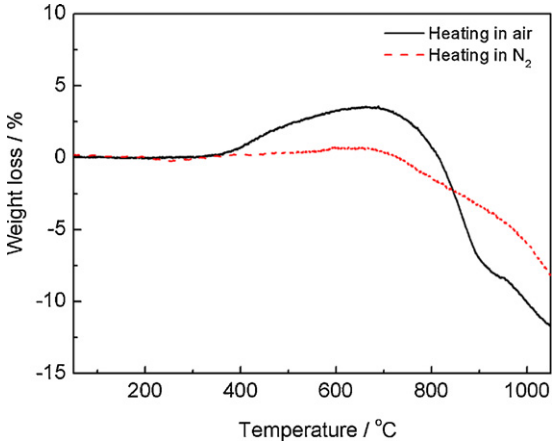

Fig. 1. TG test results for BSCF powder in air and N_2 atmospheres.

3. Results and discussion

The TG curves of the prepared BSCF powder were tested by heating in air and N_2 atmospheres, as shown in Fig. 1. In the temperature range of 400–650 °C, the TG curve obtained in the air atmosphere showed a weight increase. This weight increment can be attributed to the oxidation reaction of Co^{3+} and Fe^{3+} [16]. The total weight losses were about 11.4 wt.% in air and 8.3 wt.% in N_2 at a calcination temperature of 1000 °C. As the temperature was above 650 °C, the weight loss could be attributed to the decomposition reactions of metal nitrates and carbonate intermediates and the loss of lattice oxygen, which induced the formation of oxygen vacancies [10,11,16]. The XRD patterns of BSCF powder calcined at different temperatures are shown in Fig. 2. The as-synthesized powders show the weak crystallinity of perovskite, and there were many miscellaneous peaks in the XRD pattern. The cubic perovskite structure of single-phase BSCF was obtained via calcination at 1000 °C. SEM micrographs of the cross-section of the Ni-YSZ/YSZ/GDC/GDC-BSCF cell structure are shown in Fig. 3. These indicate that the YSZ electrolyte was dense and its thickness was ~8 μm. The YSZ electrolyte exhibited good interfacial contacts with both the Ni-YSZ electrode and the GDC barrier layer. Both the BSCF-GDC cathode and the GDC buffer-layer had porous microstructures. The cathode consists of double layers and a porous structure to assure gas diffusion. The thickness of the GDC barrier layer was ~8 μm and the thickness of BSCF-GDC layer was ~100 μm.

The cell-performance tests were executed at operating temperatures ranging from 600 to 750 °C and the results of the *I–V* and *I–P* curves are presented in Fig. 4. The maximum power densities were 191.3, 124.4, 89.1, and 57.1 mW cm^{-2} at the temperatures of 750, 700, 650, and 600 °C, respectively, with H_2 fuel and air oxidant provided at flow rates of 335 and 670 ml min^{-1}, respectively. The performance of the single cell was increased with increasing operating temperature. The OCV values of the single cell were in the range of 1.05–1.09 V, which indicates that no gas leakage occurred through the electrolyte layer of the cell. Fig. 5(a) shows the impedance spectra of the cell at different operating temperatures.

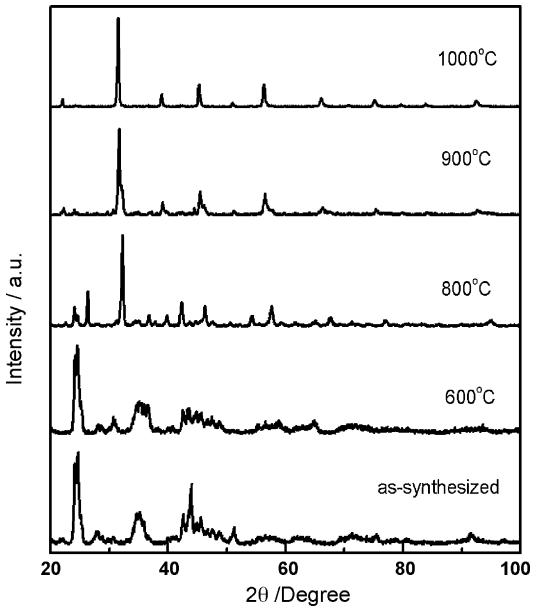

Fig. 2. XRD patterns for BSCF powders calcined at various temperatures.

The cell impedance spectra consist of two semi-circles. This indicates that at least two different electrode processes, corresponding to the high- and low-frequency arcs, occurred during molecular oxygen-reduction. According to Leng [17] and Li et al. [18,19], the high-frequency arc can be attributed to the charge-transfer of oxygen ions from electrode to the electrolyte. The low-frequency arc can be attributed to the oxygen adsorption and desorption and the diffusion of the oxygen ions on the electrode. Since the contribution of anode polarization was relatively small, the electrode resistance of the cell was thus mainly attributed to cathode polarization [17,18].

The equivalent circuit is presented in Fig. 5(b), and the fitting results using the Zview program are listed in Table 1. In the equivalent circuit, where R_E corresponds to the total ohmic resistance including the electrolyte, electrodes and the connecting-wire resistances. Here, L is the inductance, which is attributed to the Pt current–voltage probes or the high-frequency phase shift of the electrochemical equipment [17,20]. The resistance R_1 is the charge-transfer resistance, which is contributed to by the oxygen-ion transfer at the electrode-electrolyte interface and YSZ electrolyte film [13,17]. The Warburg element (W_1) is lumped with the resistances of oxygen-reduction and oxygen-ion diffusion in the cathode. The CPE_1 corresponds to the capacitance of the whole cell [18]. At 750, 700, 650, and 600 °C, the charge-transfer resistances (R_1) of the electrodes were 0.10, 0.25, 0.66, and 1.59 Ω cm^2, respectively, and the oxygen-reduction and oxygen-ion diffusion resistances (W_1) were 0.69, 0.86, 0.96, and 0.98 Ω cm^2, respectively. All types of resistance decreased with increasing temperature, indicating that the oxygen-ion transfer and the oxygen-reduction/diffusion processes were promoted with increasing temperature. Hence, these resistances of the AC-impedance test were in good agreement with the results of the performance test. The reduction of polarization resistances (R_1 and W_1) is mainly governed by the resistance of oxygen-reduction/diffusion processes (W_1) at temperatures higher than 650 °C.

Table 1
Fitting parameters from AC-impedance results obtained at different temperatures.

	Temperature (°C)			
	600	650	700	750
R_E (Ω cm^2)	4.58	3.71	3.09	2.62
R_1 (Ω cm^2)	1.59	0.66	0.25	0.10
W_1 (Ω cm^2)	0.98	0.96	0.86	0.69

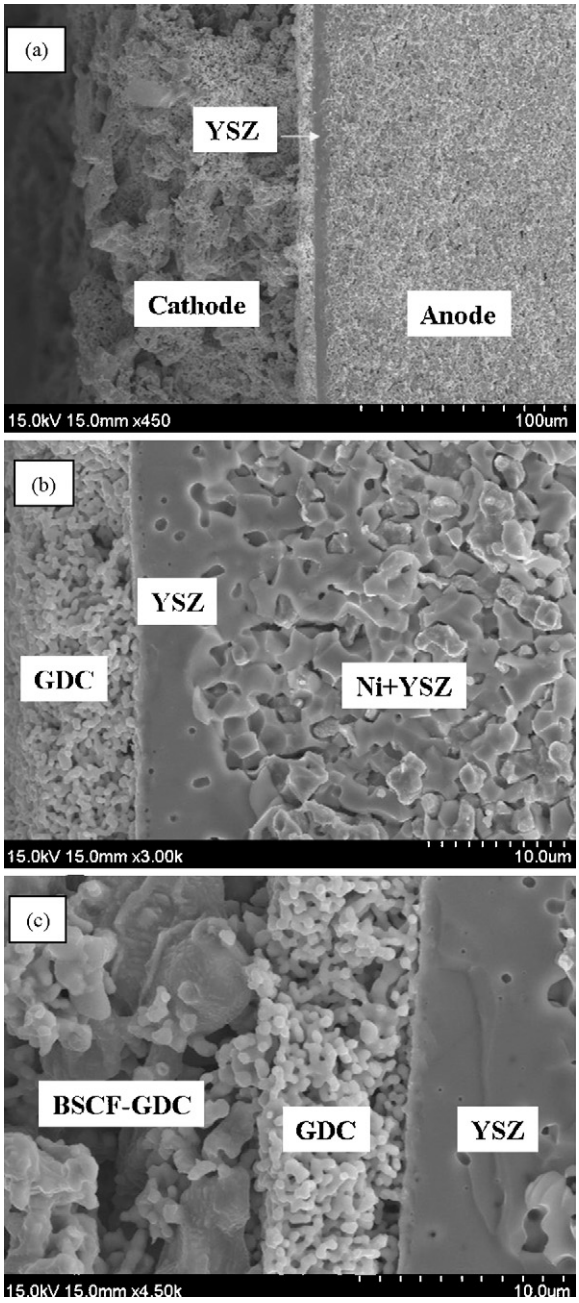

Fig. 3. SEM micrographs of the cross-sections of: (a) the whole cell; (b) part of the anode; (c) double layers of the cathode.

Fig. 6 shows the Arrhenius plot of polarization resistance for the cathode; the activation energies of the polarization resistance due to oxygen-ion transfer at the electrode/electrolyte interface (R_1) and the oxygen-reduction/oxygen-ion diffusion resistance (W_1), calculated from the slopes of the fitted lines, were 145.34 and 14.77 kJ mole^{-1}, respectively. For comparison, the activation energy for oxygen-reduction/oxygen-ion diffusion on a BSCF cathode is 88.79 kJ mole^{-1} [18]. The value is higher than that of BSCF-GDC cathode (14.77 kJ mole^{-1}), which may have resulted from the addition of a high-ionic-conductivity material (GDC) to accelerate oxygen diffusion and enhance the oxygen-ion pathway.

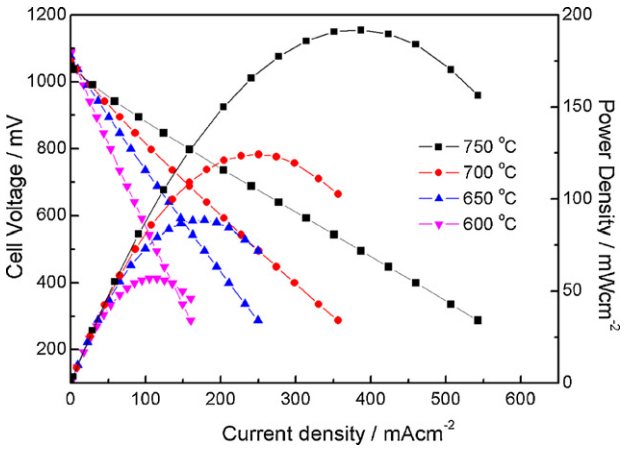

Fig. 4. Cell performance measured at different operating temperatures.

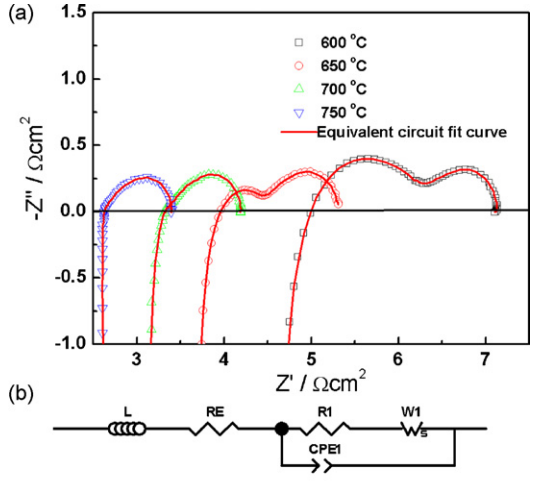

L: inductor due to Pt wire
R_E: ohmic resistance
R_1: charge-transfer resistance
W_1: oxygen-adsorption resistance
CPE_1: constant-phase element

Fig. 5. (a) Impedance spectra of unit cell at different operating temperatures. (b) Equivalent circuit.

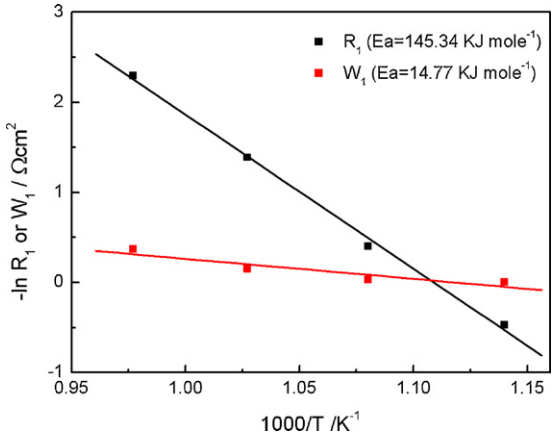

Fig. 6. Arrhenius plot of the polarization resistances (R_1 and W_1) measured at different temperatures.

4. Conclusions

BSCF-GDC synthesized via GNP is a good potential candidate for the cathode material of IT-SOFCs. The single-phase cubic perovskite structure can be obtained by powder calcination at a temperature above 1000 °C. An anode-supported single cell (Ni-YSZ/YSZ/GDC/BSCF-GDC) was fabricated and its electrochemical performance was evaluated. For the performance test of the anode-supported single cell, the maximum power densities obtained were 191.3, 124.4, 89.1, and 57.1 mW cm^{-2} at 750, 700, 650, and 600 °C, respectively. The performance of the single cell was increased at higher temperatures due to the decrease in the resistance of whole cell with increasing operating temperature. Therefore, these values of the performance test were in good agreement with the results of the AC-impedance analysis, which revealed that the oxygen-reduction reaction on the BSCF-GDC cathode is primarily limited by the oxygen-reduction/diffusion processes in the temperature range of 650–750 °C.

The BSCF-GDC composite cathode significantly improved upon the activity of the oxygen-reduction/diffusion processes compared to BSCF, yielding a notably lower activation energy than that of unmodified BSCF. The ASRs of the BSCF-GDC cathode for the charge-transfer resistance (R_1) of the electrodes were 0.10, 0.25, 0.66, and 1.59 Ω cm^2, and the oxygen-reduction and oxygen-ion diffusion resistances (W_1) were 0.69, 0.86, 0.96, and 0.98 Ω cm^2 at 750, 700, 650, and 600 °C, respectively. The activation energies of R_1 and W_1 were estimated to be approximately 145.34 and 14.77 kJ $mole^{-1}$, respectively. The BSCF-GDC composite cathode was physically and chemically compatible with the YSZ electrolyte. However, the maximum power density must be further enhanced for practical applications.

References

[1] Z. Shao, S.M. Haile, Nature 431 (2004) 170–173.
[2] G.C. Corbel, S. Mestiri, P. Lacorre, Solid State Sci. 7 (2005) 1216–1224.
[3] S. Li, Z. Lü, B. Wei, X. Huang, J. Miao, G. Gao, R. Zhu, W. Su, J. Alloys Compd. 426 (2006) 408–414.
[4] A.C. Van, M. Veen, D. Rebeilleau, C. Farrusseng, Mirodatos, Chem. Commun. 9 (2003) 32–33.
[5] S. Li, Z. Lü, X. Huang, B. Wei, W. Su, J. Phys. Chem. Solids 68 (2007) 1707–1712.
[6] Y.H. Lim, J. Lee, J.S. Yoon, C.E. Kim, H.J. Hwang, J. Power Sources 171 (2007) 79–85.
[7] F.S. Baumann, J. Maier, J. Fleig, Solid State Ionics 179 (2008) 1198–1204.
[8] H.C. Yu, F. Zhao, A.V. Virkar, K.Z. Fung, J. Power Sources 152 (2005) 22–26.
[9] L. Tan, X. Gu, L. Yang, W. Jin, L. Zhang, N. Xu, J. Membr. Sci. 212 (2003) 157–165.
[10] B. Wei, Z. Lü, S. Li, Y. Liu, K. Liu, W. Su, Electrochem. Solid-State Lett. 8 (2005) A428–A431.
[11] B. Liu, Y. Zhang, J. Alloy Compd. 453 (2008) 418–422.
[12] J. Ovenstone, J. Jung, J.S. White, D.D. Edward, S.T. Misture, J. Solid State Chem. 181 (2008) 576–586.
[13] Z. Duan, M. Yang, A. Yan, Z. Hou, Y. Dong, Y. Chong, M. Cheng, W. Yang, J. Power Sources 160 (2006) 57–64.
[14] Q. Zhu, T. Jin, Y. Wang, Solid State Ionics 177 (2006) 1199–1204.
[15] Y. Wang, S. Wang, Z. Wang, T. Wen, Z. Wen, J. Alloy Compd. 428 (2007) 286–289.
[16] S. Li, Z. Lü, X. Huang, B. Wei, W. Su, Solid State Ionics 178 (2007) 417–422.
[17] Y.J. Leng, S.H. Chan, K.A. Khor, S.P. Jiang, Int. J. Hydrogen Energy 29 (2004) 1025–1033.
[18] S. Li, Z. Lü, N. Ai, K. Chen, W. Su, J. Power Sources 165 (2007) 97–101.
[19] S. Li, Z. Lü, B. Wei, X. Huang, J. Miao, G. Cao, R. Zhu, W. Su, J. Alloy Compd. 426 (2006) 408–414.
[20] C. Fu, K. Sun, N. Zhang, X. Chen, D. Zhou, Electrochim. Acta 52 (2007) 4589–4594.